JOC The Journal of Organic Chemistry

Article

pubs.acs.org/joc

Stereoselectivity in (Acyloxy)borane-Catalyzed Mukaiyama Aldol Reactions

Joshua M. Lee,[†] Xin Zhang,[#] Per-Ola Norrby,[†,‡,§] Paul Helquist,*[,†] and Olaf Wiest*[,†]

[†]Department of Chemistry and Biochemistry, University of Notre Dame, Notre Dame, Indiana 46556, United States

[‡]Department of Chemistry and Molecular Biology, University of Gothenburg, Kemigården 4, SE 412 96 Göteborg, Sweden

[§]Pharmaceutical Technology and Development, AstraZeneca, Pepparedsleden 1, SE-431 83 Mölndal, Sweden

[#]Lab of Computational Chemistry and Drug Design, School of Chemical Biology and Biotechnology, Peking University, Shenzhen Graduate School, Shenzhen 518055, China

Supporting Information

ABSTRACT: The origin of diastereo- and enantioselectivity in a Lewis acid-catalyzed Mukaiyama aldol reaction is investigated using a combination of dispersion corrected DFT calculations and transition state force fields (TSFF) developed using the quantum guided molecular mechanics (Q2MM) method. The reaction proceeds via a closed transition structure involving a nontraditional hydrogen bond that is 3.3 kJ/mol lower in energy than the corresponding open transition structure. The correct prediction of the diastereoselectivity of a Mukaiyama aldol reaction catalyzed by the conformationally flexible Yamamoto chiral (acyloxy) borane (CAB) requires extensive conformational sampling at the transition structure, which is achieved using a Q2MM-derived TSFF, followed by DFT calculations of the low energy conformational clusters. Finally, a conceptual model for the rationalization of the observed diastereo- and enantioselectivity of the reaction using a closed transition state model is proposed.

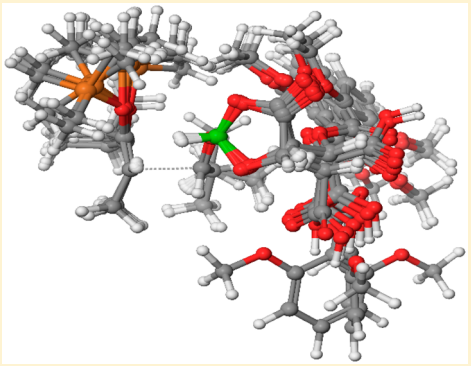

INTRODUCTION

Since their first demonstration in 1973,[1] aldol reactions of silyl enol ethers as silicon-masked enolates[2,3] have become textbook examples for the formation of carbon−carbon bonds under mild conditions with selectivity for cross-coupling products. These very commonly used reactions, an example of which is shown in Scheme 1, have become known as Mukaiyama aldol reactions. The products' resulting β-hydroxycarbonyl moiety is common in a range of synthetic targets.[4] Due to the reaction's potential to create products with two new stereocenters, the use of chiral substrates and chiral catalysts has found intense interest in the synthetic community, making the Lewis acid-catalyzed Mukaiyama aldol reaction a popular means to efficiently synthesize molecules with stereogenic centers.[5−9]

Scheme 1. General Scheme for Mukaiyama Aldol Reaction

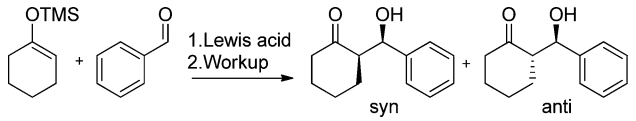

Due to the potential for catalysis of the reaction by a variety of Lewis acids[5,6,10,11] and the resulting generation of complex chiral material using relatively inexpensive chiral ligands, asymmetric catalysis of the Mukaiyama aldol reaction is an attractive topic in synthetic organic chemistry. The first example of such a reaction was reported in 1986 and used $TiCl_2$(BINOL) as a Lewis acid, resulting in low enantioselectivity.[12] Since then, many other chiral Lewis acids, including tin(II) with chiral diamine ligands[13,14] or C-2 symmetric copper(II) complexes have been investigated.[15] Figure 1 shows boron-based Lewis acids with ligands derived from inexpensive chiral pool materials, such as amino acids[16−18] or tartrate.[19]

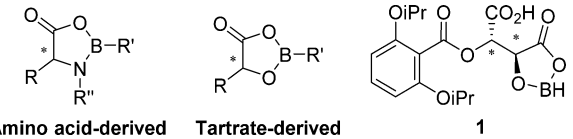

Figure 1. Amino acid (left) and tartrate (middle)-derived chiral boron Lewis acid catalysts with a specific example of chiral (acyloxy)borane catalyst **1**.

Nevertheless, a number of problems remain in the application of chiral Lewis acid catalysis to the Mukaiyama aldol reaction. The levels of diastereoselectivity and enantioselectivity can vary widely, making the choice of the appropriate Lewis acid catalyst a cumbersome, time-consuming, and scientifically unsatisfying trial-and-error process. Even in some

Received: March 20, 2016
Published: May 31, 2016

DOI: 10.1021/acs.joc.6b00594
J. Org. Chem. 2016, 81, 5314−5321

of the more successful total syntheses utilizing Lewis acid-catalyzed Mukaiyama aldol reactions that were recently reviewed,[4] enantioselectivities rarely surpass 95% e.e., and in examples where products have two stereocenters, diastereoselectivities can range from ~10:1 to essentially no selectivity, as shown in Scheme 2.[8] A systematic improvement of these results

Scheme 2. Mukaiyama Aldol Reaction Catalyzed by BF_3·OEt_2 or 1

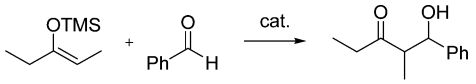

cat	d.r. (*syn*:*anti*)
BF_3·OEt_2	60:40
1	93:7

is difficult because the exact reasons for enantioselectivity in these reactions are generally not well understood, and transition state models analogous to those available to describe diastereoselectivity[20] are not available for describing enantioselectivity. Finally, the open transition states proposed for the Mukaiyama aldol reaction[20,21] and the flexibility of some of the ligands used in this reaction[19] make it difficult to predict the relevant transition states to assist in the rational design of new chiral catalysts and prediction of enantioselectivity. For example, computational studies also demonstrated the importance of transition state conformational ensembles in understanding stereoselectivity in these reactions, suggesting that an analysis of the stereoselectivity based on a single transition state might not be successful for this type of reaction.[22−24] A better understanding of the structural and conformational origin of enantio- and diastereoselectivity in such reactions is therefore highly desirable.

In 2012, we used computational methods to investigate the diastereoselectivity of Mukaiyama aldol reactions catalyzed by BCl_3.[25] The results of this study led us to conclude that the transition state of these reactions can be described by five general open transition state geometries. The work was able to rationalize several trends in the literature, including the effects of changing the silyl enol ether configuration and varying the Lewis acid catalyst.[20] The proposed models were further supported by more recent computational studies of the diastereoselectivity in the addition of an allylsilane to acetaldehyde by the Denmark group.[26]

Considering the synthetic importance of Mukaiyama aldol reactions catalyzed by chiral Lewis acids, the number of rigorous computational investigations modeling the reaction is surprisingly small, and limited information is available for the transition states of these reactions. We therefore decided to investigate the stereoselectivity, especially the enantioselectivity, of a Lewis acid-catalyzed Mukaiyama aldol reaction using computational approaches. We chose the well-characterized[27] chiral (acyloxy)borane **1** (CAB)[19] as a representative chiral Lewis acid catalyst. This catalyst has been studied in a variety of reactions and gives good to excellent enantioselectivity where the *S*,*S* catalyst predominantly produces the *S*,*S* configuration of the product shown in Scheme 2. The absolute stereochemistry of these products is supported by a total synthesis of a natural product using the catalyst.[28] The relationship of this catalyst to the BCl_3 model used in our previous studies of the diastereoselectivity of the reaction, as well as the availability of promising early trial parameters for boron in a MM2* transition state force field of a boron enolate aldol reaction,[29] make this catalyst an attractive model for the study of other catalysts that utilize transition metals.

In the computational analysis of the CAB-catalyzed Mukaiyama aldol reaction presented here, a simplified model of the CAB catalyst was initially studied using electronic structure methods to elucidate the relevant transition structures and the relationship between the reaction catalyzed by **1** and the previously studied[25] BCl_3 catalyzed reaction. These calculations were followed by computational studies of the experimentally studied system involving the full CAB ligand. Building on the findings by Morokuma and co-workers,[22] we then studied the effect of the transition state conformations on the enantioselectivity using a MM3*[30]-based transition state force field. Finally, we critically assessed the performance of Q2MM-derived TSFFs and DFT methods for the study of stereoselectivity in Mukaiyama aldol reactions.

RESULTS AND DISCUSSION

Model Studies. To develop a better understanding of the carbon−carbon bond forming, stereodetermining transition state in the CAB-catalyzed Mukaiyama aldol reaction, a model system using a simplified, achiral catalyst (Scheme 3) was

Scheme 3. Molecules Used as a Training Set for the Q2MM Parameterization of a TSFF for the CAB-Catalyzed Mukaiyama Aldol Reaction

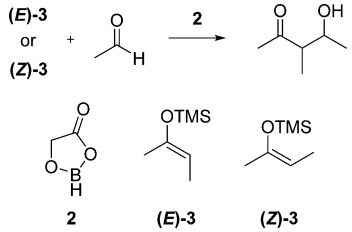

initially studied. The model catalyst, **2**, was simplified compared to the experimentally used catalyst, **1**, by substituting the carbon stereocenter on the five-membered ring with a methylene group. First, an initial series of calculations studied the different transition structures of the reactions of both isomers of the enol silyl ether, **3**, and acetaldehyde, catalyzed by **2**, leading to the *syn* and *anti* products, using B3LYP-D3/6-31G* calculations with the THF solvent used in these reaction represented by an implicit IEFPCM solvent model.

For the reaction of (*Z*)-**3** with acetaldehyde, the open pro-*anti* and pro-*syn* transition structures had no energy difference within computational uncertainty. These transition states are shown in Figure 2. In analogy to the transition structures reported for the BF_3-catalyzed reaction,[20] the forming carbon−carbon bond has long calculated bond lengths of 2.1−2.2 Å, depending on the conformation, indicating an early transition state. These result are consistent with the reported lack of diastereoselectivity observed for catalysis by BF_3, but the *syn* selectivity reported with the CAB catalyst[19] warranted further investigation. It is worth noting that in these transition structures, the α-carbon atom in **2** that is analogous to a carbon stereocenter in **1** is pointing away from the other atoms, making it difficult to explain the experimentally observed enantioselectivity of the reaction. Based on the discrepancy between these calculations describing an open transition structure and the stereoselectivity induced by the catalyst, the

DOI: 10.1021/acs.joc.6b00594
J. Org. Chem. 2016, 81, 5314−5321

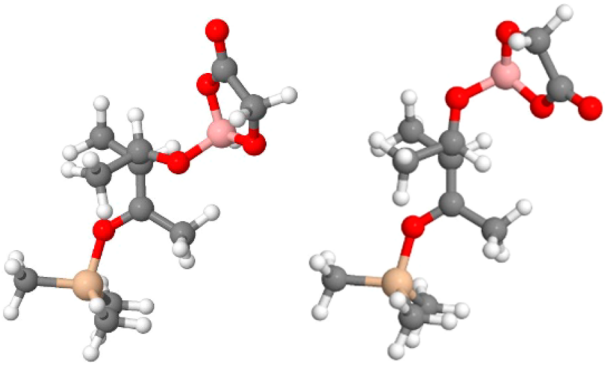

Figure 2. Open transition structures for the reaction of (*Z*)-**3** with acetaldehyde catalyzed by **2**. (Left) Pro-*syn* transition structure. (Right) Pro-*anti* transition structure.

possibility of alternative transition structures having other interactions warranted further investigation.

To investigate alternative transition structures, we started from the well-documented trend of aldehyde hydrogens to undergo hydrogen bonding with suitable hydrogen bond acceptors in the transition states of several reaction classes, including examples of aldol reactions.[31−34] This trend led us to investigate less conventional hydrogen bonding interactions. While we were unable to locate transition structures involving the aldehyde hydrogen, manual conformational searches did locate transition structures with an interaction with distances of ∼2.4 Å between an oxygen on model catalyst **2** and the vinylic hydrogen of (*Z*)-**3**, leading to both the *syn* (Figure 3a, left) and the *anti* (Figure 3a, right) products. Transition structure optimizations often led to structures in which either of the oxygen atoms of the five-membered ring in the model catalyst **2** formed interactions with the vinylic hydrogen on the α-carbon of the silyl enol ether, forming a closed transition state. Two examples of this type of transition structure are shown in Figure 3b for the reaction of (*E*)-**3** with acetaldehyde leading to the *syn* (Figure 3b, left) and the *anti* (Figure 3b, right) products. In the calculations describing these interactions, the distances range from 2.3 to 3.0 Å, and the interactions do not always fit the traditional description of a hydrogen bond.[35] While nontraditional hydrogen bonds to aldehyde hydrogens and hydrogens on aromatic rings are known in other reactions, to the best of our knowledge, this nontraditional hydrogen bond to a vinylic hydrogen of an enol derivative has not previously been described in the literature.

The formation of a closed transition state by this interaction leads to a six-membered ring in which the substituents can be positioned in either axial or equatorial position. We studied the possible combinations of pseudoaxial and pseudoequatorial substituent positions, shown in Figure 4, leading to the two diastereomers, each of which can form as either of two enantiomers. Within these groups, transition structures can adopt several conformations including several positions of the five-membered ring of the catalyst relative to the six-membered ring. The position of the catalyst was changed to be proximal or distal to the pseudoaxial substituent of the silyl enol ether and to coordinate to the α-hydrogen on the silyl enol either via its carboxylate oxygen or alkoxide oxygen. While most transition structures were located, some structures contained unfavorable interactions and could not be located. A summary of structures is provided in Table S1 of the Supporting Information, together with the pertinent coordinates. The results show that the

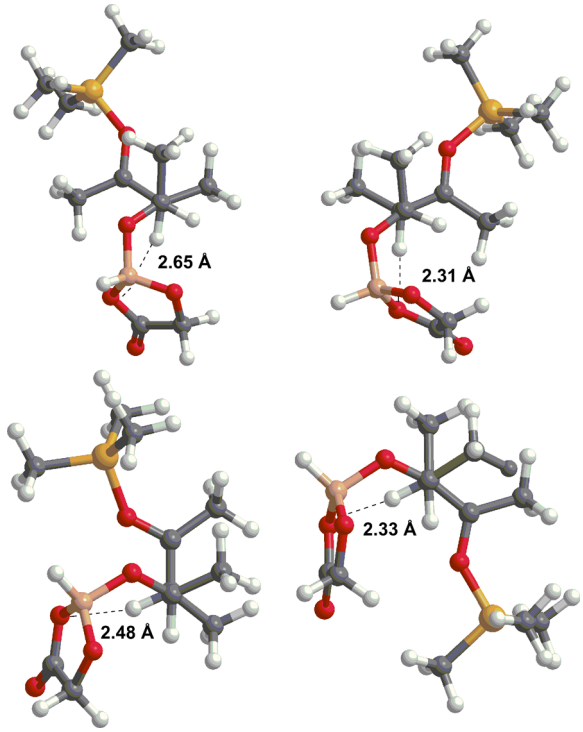

Figure 3. (a) Closed transition structures for the reaction of (*Z*)-**3** with acetaldehyde, catalyzed by **2** with nontraditional oxygen−hydrogen bond highlighted with dashed lines. (Left) Representative pro-*syn* transition structure. (Right) Representative pro-*anti* transition structure. (b) Transition structures for the reaction of (*E*)-**3** with acetaldehyde, catalyzed by **2** with oxygen−hydrogen interactions highlighted. (Left) Representative pro-*syn* closed transition structure. (Right) Representative pro-*anti* closed transition structure.

aldehyde substituent preferentially adopts a pseudoequatorial position. This observation can be attributed to the electronically disfavored coordination of the boron atom *trans* to the aldehyde hydrogen. This preference significantly limits the conformational possibilities of the transition state.

Studies of the CAB-Catalyzed Reaction. An important consequence of the closed transition structure is that the conformations shown in Figure 4 are clearly important, but limited in number compared to the possibility of an open transition structure. At the same time, the large number of freely rotatable bonds in the CAB ligand as well as the precedents in the literature[22] indicate that more extensive conformational sampling will be required.

A number of different diastereomers need to be considered, in addition to the large conformational space for each pathway. Because the silyl enol ether and aldehyde each contain two nonequivalent faces, and the boron atom in the catalyst forms a stereocenter upon coordination to the aldehyde, eight possible diastereomeric transition state configurations have to be modeled. These transition state configurations are labeled using generic terms TS1−TS8, as defined in Figure 5 and in which the transition structure is shown in the open form for clarity. Based on the chirality of the catalyst being modeled and the experimental work by Furuta et al.,[19] the reaction being studied should be *syn* selective (TS1,TS3, TS6, TS8), and the *syn* product should predominantly have an (*S*,*S*) configuration (TS1, TS8). It is clear that the combination of eight possible transition structures, each needing extensive conformational sampling at the transition structure, is not practical for the

DOI: 10.1021/acs.joc.6b00594
J. Org. Chem. 2016, 81, 5314−5321

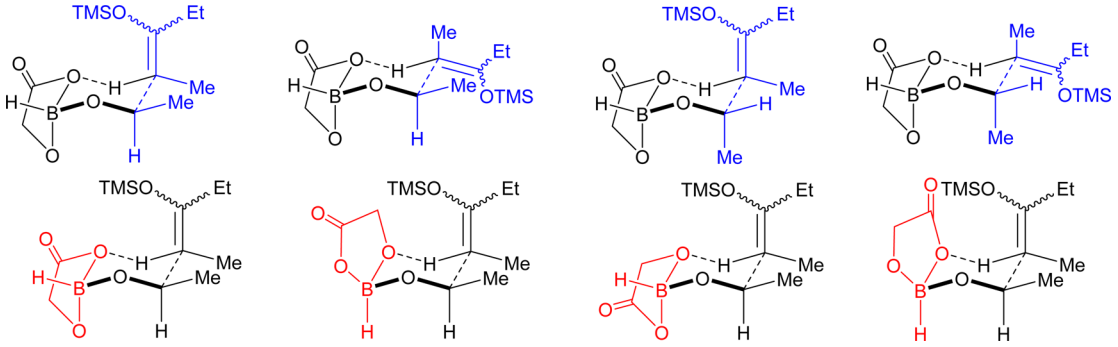

Figure 4. Representations for different closed transition structures. Blue highlighting is used to emphasize conformational changes relating to the silyl enol ether and aldehyde part of the transition states. Red highlighting is used to emphasize conformational changes relating to the (acyloxy)borane part of the transition states. The same structure is used on the far left in both rows to serve as a common point of reference.

	1	2	3
TS1	S	S	R
TS2	R	S	R
TS3	R	R	R
TS4	S	R	R
TS5	S	R	S
TS6	R	R	S
TS7	R	S	S
TS8	S	S	S

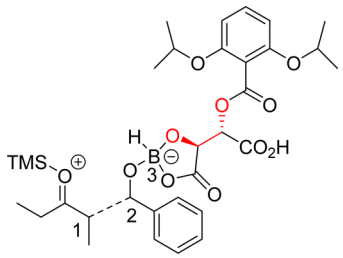

Figure 5. Stereoisomeric transition structures. Different diastereomeric pathways are labeled TS1−TS8. Stereocenters that can vary in the transition state are labeled 1−3. The stereocenters of the catalyst are highlighted in red.

standard approach of manually constructing starting geometries for the transition structures, followed by optimization.

We therefore envisioned an approach to this problem that is based on our earlier work on the generation of transition state force fields (TSFF) using the quantum-guided molecular mechanics (Q2MM) method.[36−39] The transition structures calculated in the model system can be used to train a TSFF, which would then allow rapid and extensive conformational sampling. The relevant low-energy conformations of the different transition states were in earlier applications[37−39] used to directly calculate the diastereo- and enantioselectivity of the reaction after Boltzmann averaging, as described previously. Alternatively, the results of the conformational search at the transition state could be used as input for electronic structure calculations, thus allowing accurate electronic structure calculations of a limited number of structures that are representative of the much larger conformational space. Most of the important rotatable bonds and stereocenters are far away from the reaction center and can be described by standard force field parameters. We therefore hypothesized that the parametrization of the TSFF should be straightforward and that even a first-order TSFF should provide a sufficient sampling of the conformational space for the different transition states.

The reaction shown in Scheme 2 was studied because the same substrates had been used with $BF_3{\cdot}OEt_2$ as a catalyst,[20] the substrates were similar to those used in the force field training set, and the reaction was more stereoselective than other aldol reactions with the same catalyst.[19] The training set for the TSFF includes 10 structures derived from the QM investigation. Closed transition structures included various catalyst positions and diasteromeric configurations, along with an open pro-*anti* transition structure. The complete training set is provided in the Supporting Information (Table S1). In order to allow the force field to describe reactions with aromatic aldehydes, the methyl group of acetaldehyde in each structure from the QM investigation was replaced with a phenyl group, and the structures were reoptimized to transition structures (Table S2). Both sets of transition structures were used as a training set for the TSFF. For detailed information about the fitting procedures and final TSFF parameters, see the Supporting Information.

The force field thus obtained was first validated by comparing QM transition structure optimizations to the results of the MM optimizations using the TSFF. One way to visualize agreement between the QM and MM data is by overlaying the structures produced by their respective optimizations. Two examples of such overlays for the reaction of benzaldehyde with the TMS enol ether of diethylketone are shown in Figure 6.

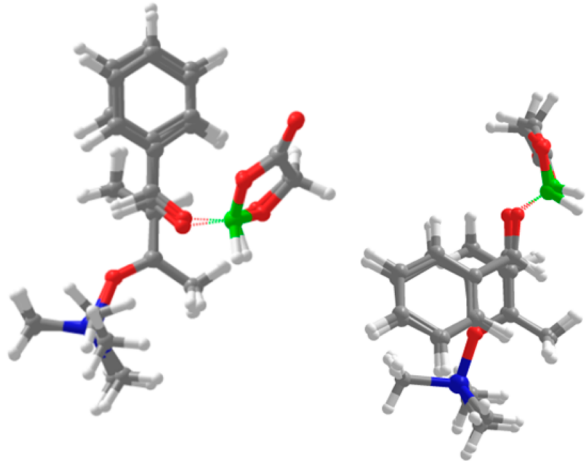

Figure 6. Overlay of MM and QM optimized transition structures for the CAB-catalyzed Mukaiyama aldol reaction.

Visual inspection and numerical comparison of key structural parameters (including partial charges, bond lengths, angles etc., see Charts S1, S2 in the Supporting Information) indicate that the force field accurately models the CAB-catalyzed Mukaiyama aldol reaction. The Hessian matrix elements between MM and QM calculations (Chart S3 in the Supporting Information) also show reasonable agreement. While many of the Hessian matrix data points align with the *x*-axis, those points are not described by the force field and cannot be fit using our current methods.[38] The outliers in the plot having MM values near 700 $kJmol^{-1}$ $Å^{-2}amu$ are a consequence of the treatment of the transition

DOI: 10.1021/acs.joc.6b00594
J. Org. Chem. 2016, 81, 5314−5321

state as a minimum in TSFFs, as described in the methods section.[38] Most importantly, the force field replicates the relative energies between the training set structures well (Chart S4 in the Supporting Information). This indicates that the relative MM and QM energies agree in the training set and that the overall goal of the force field, the accurate calculation of the conformational and diastereomeric transition state energy differences, is achievable.

With the validated TSFF in hand, an extensive conformational sampling of the eight possible transition states shown in Figure 5 for the experimentally studied reaction shown in Figure 2, including the full CAB catalyst **1**, was performed using 35,000 Monte Carlo steps and a GBSA solvent model in MacroModel (for command files including parameters chosen, see the Supporting Information). The results of this conformational sampling were analyzed in three different ways. First, the full set of conformations calculated by the TSFF was used to calculate the *syn*/*anti* diastereoselectivity as well as the (*S*,*S*):(*R*,*R*) enantioselectivity for the experimentally observed *syn* product of the reaction[18,25] through Boltzmann averaging using the relative energies of the different transition structures from the TSFF. Second, the number of conformations was reduced to the chemically relevant structures by clustering using a 12 kJ/mol energy window and a geometry RMSd filter (for details, see Supporting Information) and calculation of the stereochemical distribution as above. Finally, the relevant conformations from the clustering were reoptimized to transition structures at the M06-2X/6-31G* + level of theory using the IEFPCM implicit solvent model. The Gibbs free energies were then used in the Boltzmann averaging (for optimized geometries and energies, see Supporting Information).

"MM" includes all structures after the full MM minimization. "MM clustered" only includes the lowest energy structure in each cluster. "QM" includes the same set of structures as "MM clustered." Experimental values are from Furuta et al.[19,27]

The results of these analyses are summarized in Table 1. The full set of results of the conformational search using the TSFF predicts the correct enantiomer of the *syn* product. However, the first-generation force field does not accurately quantify the e.r. in this reaction and differs by a factor of ∼10. Also, the predictions indicate the incorrect diastereomer. In the MM calculations, this lack of agreement appears to be in part due to error in the potential about the torsion about the boron−oxygen coordination, which was difficult to define in the MM3* force field. Also, through-space interactions are not fully parametrized in the current Q2MM methodology, which contributes to the error.

Table 1. Stereoselectivity Determinations Based on Different Methods

method	*syn*/*anti*	(*S*,*S*):(*R*,*R*)
MM	0.7	2.6
MM clustered	0.7	2.2
QM	14.2	1555
experiment	16	24

However, structural properties of the ensembles of conformations still provide information about the enantioselecitvity of the reaction because the TSFF force field was developed based on the Hessian matrix of a QM training set and should be able to reproduce the geometries of saddle points on the potential energy surface. In particular, the torsion of the bond of the catalyst located between two vicinal stereocenters likely influences stereoselectivity by controlling the position of the bulky part of the chiral catalyst. We therefore reasoned that the structures, but not the relative energies, were reproduced by the first generation TSFF. Thus, a more thorough investigation of the diastereomeric transition state pathways was performed. For this, the number of structures to be calculated was reduced to unique and chemically relevant conformations using clustering. Between 11 and 30 conformations were identified for each of the eight transition states shown in Figure 5. As shown in Table 1 and the Supporting Information, the clustered conformational ensemble produced essentially the same stereochemical prediction as the full set of structures (for coordinates of conformational ensembles for each transition structure after clustering, see Supporting Information). Therefore, the much smaller set of structures after the clustering calculation could be optimized using M06-2X while still retaining the important conformations. Although the remainder of this study will focus on the DFT results, it is important to note that relevant conformers of the transition states could not have been located without developing the TSFF, which then feeds back into electronic structure calculations. This type of iterative approach can leverage the higher accuracy of the QM calculations with the speed of conformational searching at the force field level.

It is gratifying to note that the conformational ensemble not only predicts the correct diastereomer and enantiomer of the product, but also gives a diastereoselectivity that is in quantitative agreement with the experimental value. However, the enantioselectivity of the reaction is overestimated by a factor of ∼65, corresponding to an error of ∼7 kJ/mol, which is larger than the ∼2−3 kJ/mol error typically observed in e.e. predictions of enantioselectivity using TSFFs.[38,39] Although there are several possible reasons for this, one key difference between the systems studied here and the reactions studied earlier is the large degree of zwitterionic character of the transition state, making the treatment of solvent effects by implicit models difficult.

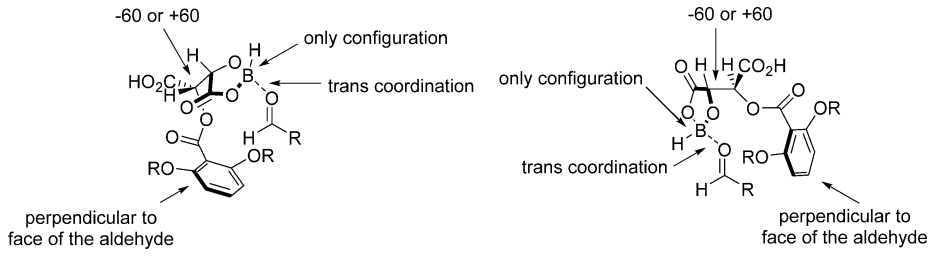

Figure 7. Two preferred catalyst positions relative to the aldehyde.

DOI: 10.1021/acs.joc.6b00594
J. Org. Chem. 2016, 81, 5314−5321

Maybe more importantly, the QM data were useful in identifying structural trends in the lowest energy conformations. One observation from the results of the conformational analysis is a strong preference for the boron stereocenter to have the *S* configuration seen in TS5−TS8, rather than the *R* configuration in TS1−TS4. QM calculations indicate the disfavored configuration to be more than 70 kJ/mol less stable than the favored configuration and therefore negligible (see Supporting Information). This finding simplifies further analysis by allowing it to be limited to four rather than eight diastereomeric pathways.

The bulk of the CAB catalyst is preferentially positioned approximately perpendicular to the plane of the aldehyde. The MM optimization with the TSFF incorrectly places the bulk of the catalyst in front of a face of the aldehyde, but the QM reoptimization corrects this positioning, emphasizing the importance of through-space interactions that are not part of the TSFF parametrization.

Figure 7 summarizes the results of the structural analysis of the eight transition structures and their conformational preferences. Combining the preferred configuration of the boron stereocenter, the preferred torsion angles about the bond between the two stereocenters of the catalyst, and the preference for the Lewis acid to coordinate *trans* to the aldehyde hydrogen leads to two main catalyst positions that influence enantioselectivity. Based on these preferences, the bulk of the ligand is positioned proximal to the rest of the aldehyde. This positioning is unlikely to be caused by a through-space, Coulombic stabilization of the electrophilic carbon of the aldehyde by the carboxylate because experimental studies have shown that if the acid is methylated, the catalyst can still promote enantioselectivity in these reactions.[19,27] Based on the results discussed for the model system, it is more likely that there is a preference for one oxygen atom of the acyloxyborane to form a nontraditional hydrogen bond with a hydrogen atom on the nucleophile or aldehyde, thus differentiating the enantiotopic faces of the aldehyde. However, experimental studies will be necessary to confirm or disprove this hypothesis.

CONCLUSIONS

The acyloxyborane-catalyzed Mukaiyama aldol reaction was found to proceed via a closed transition structure involving a nontraditional hydrogen bond between one of the oxygens on the acyloxyborane ring and a hydrogen on the enolate double bond. This closed transition structure was calculated to be 3.3 kJ/mol more stable than the open transition structure more commonly invoked in the Mukaiyama aldol reaction. These results rationalize the fact that chiral acyloxyboranes induce good to very good enantioselectivity despite the chiral center being far removed from the forming carbon−carbon bond.

The problem of understanding the conformationally flexible CAB ligands, such as the one introduced by Yamamoto, in a transition state can be addressed by a novel approach where extensive sampling of the transition state conformations is performed using a first-order transition state force field, which is generated using the Q2MM approach. After clustering of the multiple transition structure conformations and recalculation of the relative energies using dispersion-corrected DFT methods with an implicit solvent model, very good agreement between the experimental and computational diastereoselectivity is achieved. The results demonstrate the importance of multiple transition state conformations for the stereochemical outcome of the reaction.[22−24] They provide a rigorous and clear protocol to generate and study the relevant conformations that are complementary to the AFIR method,[22,23] which uses electronic structure methods for the conformational search, in that the Q2MM code is freely available and the TSFF, once generated, allows a rapid and comprehensive exploration of the conformational space. Finally, the conceptual model developed here to explain the observed conformational preferences could aid in the selection of substrates and the design of new chiral catalysts for Mukaiyama aldol reactions, including enantioselective reactions, in general. We expect that the methods of this study can be similarly applied to other stereoselective reactions.

COMPUTATIONAL METHODS

QM Calculations. All QM calculations were performed using Gaussian 09.[40] Optimizations of the model system were at the B3LYP/6-31G* level of theory with Grimme dispersion corrections (empirical dispersion = gd3bj)[41,42] and an implicit IEFPCM solvation model[43] with solvent parameters chosen to represent tetrahydrofuran, while reoptimization of the transition structures from the conformational search of the CAB ligand were done at the M06-2X/6-31G* level of theory with the same implicit IEFPCM solvation model. Charge data were obtained by using the pop = (chelpg,dipole) option.[44] Transition structures reported are optimized without constraints, and their identities were confirmed by harmonic frequency analysis and visual inspection of the imaginary frequency. The frequency calculations were also used to obtain the Hessian matrix elements and the thermal corrections to the energies, which are reported as free Gibbs energies in kJ/mol.

Transition State Force Field Development. The transition state force field was developed using methods described previously.[36,45,46] All force fields designed in this paper were created as substructure-specific parameter sets appended to the MM3* force field. The method was modified to include a GBSA solvent model[47] in all MM calculations during the Q2MM optimization.

The parameters for the atoms in the MM3* substructure shown in the macromodel substructure file in the Supporting Information were subjected to the Q2MM reparameterization procedure. The substructure is designed to recognize (acyloxy)borane-coordinated carbonyl moieties that have a zero-order bond to a silyl enol ether. The parameters that were optimized include bond equilibrium distances, bond force constants, dipole constants, bend equilibrium distances, bend force constants, and torsion parameters. The quality of the parameters was determined by comparing QM and MM calculations for point charges, structural elements, Hessian elements, and relative conformational energy. Detailed parametrization information is available in the Supporting Information.

Prior to running the Q2MM program, the Hessian matrices of each QM training structure were modified to replace each transition structure's negative eigenvalue corresponding to the reaction coordinate with a large positive eigenvalue.[45] This approach allows the transition structures to be modeled as ground-state structures.

Conformational Search. The TSFF was used to perform a conformational search of the highly flexible transition structures. Because the two reacting carbons and the boron form three stereogenic centers in the transition state, eight separate conformational searches were necessary for the system in order to investigate all possible diastereomeric pathways. Nine rotatable bonds were sampled during conformational searches using the low-mode conformation search[48] option in MacroModel. Thirty five thousand steps were taken, and a GBSA solvent model for chloroform was included. The electrostatics were treated using the default extended nonbonded interaction cutoff options, a cutoff of 89.4427 Å for charge-dipole interactions, and a cutoff of 999999 Å for charge−charge interactions. Comparison atoms included all non-hydrogen atoms except for the carbons attached to silicon. Conformer elimination was performed by considering conformers to be redundant if all comparison atoms were within 0.5 Å for two conformers. Minimization was performed using

DOI: 10.1021/acs.joc.6b00594
J. Org. Chem. 2016, 81, 5314−5321

the truncated Newton conjugate gradient (TNCG) method[49] with a limit set to 500 steps. The resulting structures were reoptimized in the TSFF using the TNCG method for an additional 1500 steps, including the same conformer elimination settings as in the conformational search. MarcoModel command files for this study are in the Supporting Information.

The remaining conformations were limited to an energy window of 12 kJ/mol. Using the script for clustering of conformers included in MacroModel, RMSD matrices were calculated for the resulting structures, and the conformers were clustered using the average linkage clustering method. For the RMSD matrix, all heavy atoms were included, except for the entire TMS group, the carbonyl oxygen of the benzoate ester, the entire aryl group of the catalyst, and all unsubstituted aryl carbons on benzaldehyde. Only the lowest energy structure for each cluster was saved because the higher energy structures within each cluster were determined to be very structurally similar to the lowest energy structure.

■ ASSOCIATED CONTENT

Supporting Information

The Supporting Information is available free of charge on the ACS Publications website at DOI: 10.1021/acs.joc.6b00594.

Additional computational data, including coordinates and energies for all described transition structures. The Q2MM code is freely available via GitHub at https://github.com/q2mm/q2mm(PDF)

Training set structures used for Q2MM optimization (ZIP)

Transition states with (*Z*)-**3** (ZIP)

Results MM conformational search corresponding to "MM Clustered" (ZIP)

Results QM conformational search corresponding to "MM Clustered" (ZIP)

Transition states with (*E*)-**3** (ZIP)

■ AUTHOR INFORMATION

Corresponding Authors

*phelquis@nd.edu

*Olaf.G.Wiest.1@nd.edu

Notes

The authors declare no competing financial interest.

■ ACKNOWLEDGMENTS

We thank the U.S. National Science Foundation (NSF CHE1058075), the Shenzhen Peacock Program (JCYJ20140509093817689), the National Research Council of Sweden (grant no. 2010-4856), and Astra-Zeneca for financial support and the TeraGrid (TG-CHE120050) and the Notre Dame Center for Research Computing for computational resources. J.M.L. thanks the Chemistry Biochemistry Biology Interface (CBBI) Program funded by NIH Training Grant T32GM075762 for a predoctoral fellowship.

■ REFERENCES

(1) Mukaiyama, T.; Narasaka, K.; Banno, K. *Chem. Lett.* **1973**, 1011.

(2) Saigo, K.; Osaki, M.; Mukaiyama, T. *Chem. Lett.* **1975**, 989.

(3) Gennari, C.; Bernardi, A.; Cardani, S.; Scolastico, C. *Tetrahedron Lett.* **1985**, *26*, 797.

(4) Kan, S. B.; Ng, K. K.; Paterson, I. *Angew. Chem., Int. Ed.* **2013**, *52*, 9097.

(5) Geary, L. M.; Hultin, P. G. *Tetrahedron: Asymmetry* **2009**, *20*, 131.

(6) Palomo, C.; Oiarbide, M.; Garcia, J. M. *Chem. Soc. Rev.* **2004**, *33*, 65.

(7) Beutner, G. L.; Denmark, S. E. *Angew. Chem., Int. Ed.* **2013**, *52*, 9086.

(8) Matsuo, J.; Murakami, M. *Angew. Chem., Int. Ed.* **2013**, *52*, 9109.

(9) Fu, K.; Zheng, J.; Liu, X.; Feng, X.; Lin, L. *Chem. Commun.* **2015**, *51*, 3106.

(10) Machajewski, T. D.; Wong, C. H. *Angew. Chem., Int. Ed.* **2000**, *39*, 1352.

(11) Denmark, S. E.; Stavenger, R. A. *Acc. Chem. Res.* **2000**, *33*, 432.

(12) Reetz, M. T.; Kyung, S. H.; Bolm, C.; Zierke, T. *Chemistry & Industry* **1987**, *18*, 824.

(13) Kobayashi, S.; Mukaiyama, T. *Chem. Lett.* **1989**, 297.

(14) Kobayashi, S.; Uchiro, H.; Fujishita, Y.; Shiina, I.; Mukaiyama, T. *J. Am. Chem. Soc.* **1991**, *113*, 4247.

(15) Evans, D. A.; Murry, J. A.; Kozlowski, M. C. *J. Am. Chem. Soc.* **1996**, *118*, 5814.

(16) Parmee, E. R.; Tempkin, O.; Masamune, S.; Abiko, A. *J. Am. Chem. Soc.* **1991**, *113*, 9365.

(17) Kiyooka, S.; Kaneko, Y.; Komura, M.; Matsuo, H.; Nakano, M. *J. Org. Chem.* **1991**, *56*, 2276.

(18) Corey, E. J.; Cywin, C. L.; Roper, T. D. *Tetrahedron Lett.* **1992**, *33*, 6907.

(19) Furuta, K.; Maruyama, T.; Yamamoto, H. *J. Am. Chem. Soc.* **1991**, *113*, 1041.

(20) Heathcock, C. H.; Davidsen, S. K.; Hug, K. T.; Flippin, L. A. *J. Org. Chem.* **1986**, *51*, 3027.

(21) Denmark, S. E.; Lee, W. S. *J. Org. Chem.* **1994**, *59*, 707.

(22) Hatanaka, M.; Maeda, S.; Morokuma, K. *J. Chem. Theory Comput.* **2013**, *9*, 2882.

(23) Sameera, W. M. C.; Hatanaka, M.; Kitanosono, T.; Kobayashi, S.; Morokuma, K. *J. Am. Chem. Soc.* **2015**, *137*, 11085.

(24) Lopez, C. S.; Alvarez, R.; Vaz, B.; Faza, O. N.; de Lera, A. R. *J. Org. Chem.* **2005**, *70*, 3654.

(25) Lee, J. M.; Helquist, P.; Wiest, O. *J. Am. Chem. Soc.* **2012**, *134*, 14973.

(26) Wolf, L. M.; Denmark, S. E. *J. Am. Chem. Soc.* **2013**, *135*, 4743.

(27) Furuta, K.; Shimizu, S.; Miwa, Y.; Yamamoto, H. *J. Org. Chem.* **1989**, *54*, 1481.

(28) Sato, M.; Sunami, S.; Sugita, Y.; Kaneko, C. *Chem. Pharm. Bull.* **1994**, *42*, 839.

(29) Bernardi, A.; Capelli, A. M.; Gennari, C.; Goodman, J. M.; Paterson, I. *J. Org. Chem.* **1990**, *55*, 3576.

(30) Lii, J. H.; Allinger, N. L. *J. Am. Chem. Soc.* **1989**, *111*, 8566.

(31) Corey, E. J.; Rohde, J. J. *Tetrahedron Lett.* **1997**, *38*, 37.

(32) Corey, E. J. *Angew. Chem., Int. Ed.* **2002**, *41*, 1650.

(33) Wong, M. W. *J. Org. Chem.* **2005**, *70*, 5487.

(34) Paddon-Row, M. N.; Anderson, C. D.; Houk, K. N. *J. Org. Chem.* **2009**, *74*, 861.

(35) Bernstein, J.; Davis, R. E.; Shimoni, L.; Chang, N. L. *Angew. Chem., Int. Ed. Engl.* **1995**, *34*, 1555.

(36) Norrby, P. O.; Liljefors, T. *J. Comput. Chem.* **1998**, *19*, 1146.

(37) Donoghue, P. J.; Helquist, P.; Norrby, P. O.; Wiest, O. *J. Chem. Theory Comput.* **2008**, *4*, 1313.

(38) Lime, E.; Lundholm, M. D.; Forbes, A.; Wiest, O.; Helquist, P.; Norrby, P. O. *J. Chem. Theory Comput.* **2014**, *10*, 2427.

(39) Donoghue, P. J.; Helquist, P.; Norrby, P. O.; Wiest, O. *J. Am. Chem. Soc.* **2009**, *131*, 410.

(40) Frisch, M. J.; Trucks, G. W.; Schlegel, H. B.; Scuseria, G. E.; Robb, M. A.; Cheeseman, J. R.; Scalmani, G.; Barone, V.; Mennucci, B.; Petersson, G. A.; Nakatsuji, H.; Caricato, M.; Li, X.; Hratchian, H. P.; Izmaylov, A. F.; Bloino, J.; Zheng, G.; Sonnenberg, J. L.; Hada, M.; Ehara, M.; Toyota, K.; Fukuda, R.; Hasegawa, J.; Ishida, M.; Nakajima, T.; Honda, Y.; Kitao, O.; Nakai, H.; Vreven, T.; Montgomery, J. A., Jr., Peralta, J. E.; Ogliaro, F.; Bearpark, M.; Heyd, J. J.; Brothers, E.; Kudin, K. N.; Staroverov, V. N.; Kobayashi, R.; Normand, J.; Raghavachari, K.; Rendell, A.; Burant, J. C.; Iyengar, S. S.; Tomasi, J.; Cossi, M.; Rega, N.; Millam, J. M.; Klene, M.; Knox, J. E.; Cross, J. B.; Bakken, V.; Adamo, C.; Jaramillo, J.; Gomperts, R.; Stratmann, R. E.; Yazyev, O.; Austin, A. J.; Cammi, R.; Pomelli, C.; Ochterski, J. W.; Martin, R. L.; Morokuma, K.; Zakrzewski, V. G.; Voth, G. A.; Salvador, P.;

DOI: 10.1021/acs.joc.6b00594
J. Org. Chem. 2016, 81, 5314−5321

Dannenberg, J. J.; Dapprich, S.; Daniels, A. D.; Farkas, Ö.; Foresman, J. B.; Ortiz, J. V.; Cioslowski, J.; Fox, D. J. *Gaussian 09, R. A.*; Gaussian, Inc.: Wallingford CT, 2009.
(41) Grimme, S.; Ehrlich, S.; Goerigk, L. *J. Comput. Chem.* **2011**, *32*, 1456.
(42) Grimme, S.; Antony, J.; Ehrlich, S.; Krieg, H. *J. Chem. Phys.* **2010**, *132*, 19.
(43) Tomasi, J.; Mennucci, B.; Cammi, R. *Chem. Rev.* **2005**, *105*, 2999.
(44) Breneman, C. M.; Wiberg, K. B. *J. Comput. Chem.* **1990**, *11*, 361.
(45) Norrby, P. O. *J. Mol. Struct.: THEOCHEM* **2000**, *506*, 9.
(46) Hansen, E.; Rosales, A. R.; Tutkowski, B.; Norrby, P. O.; Wiest, O. *Acc. Chem. Res.* **2016**, *49*, 996.
(47) Bashford, D.; Case, D. A. *Annu. Rev. Phys. Chem.* **2000**, *51*, 129.
(48) Kolossvary, I.; Guida, W. C. *J. Am. Chem. Soc.* **1996**, *118*, 5011.
(49) Ponder, J. W.; Richards, F. M. *J. Comput. Chem.* **1987**, *8*, 1016.

NOTE ADDED AFTER ASAP PUBLICATION

Due to a production error (a distance measurement was missing), Figure 3 was replaced on June 14, 2016.

DOI: 10.1021/acs.joc.6b00594
J. Org. Chem. 2016, 81, 5314−5321